Molding of Reflection and Scattering from Uniform Walls Using Space-Periodic Metasurfaces

S. Kosulnikov, F. S. Cuesta, X. Wang, and S. A. Tretyakov, *Fellow, IEEE*

***Abstract*—Active development is taking place in reconfigurable and static metasurfaces that control and optimize reflections. However, existing designs typically only optimize reflections from the metasurface panels, neglecting interference with reflections originating from supporting walls and nearby objects. In this study, we investigate how engineering the metasurface properties can modify the total scattering pattern, enabling the modification and optimization of reflections from significantly larger illuminated areas than the metasurface panel. To accomplish this, a general design approach is developed to create periodical metasurfaces with controlled reflection phase and amplitude for all propagating Floquet harmonics. By combining metasurface reflections with those from the surrounding walls, the total scattering can be manipulated. The study demonstrates how appropriately designed metasurfaces can modify reflections from surrounding walls, enhancing the functionalities of metasurfaces. These findings are intended to facilitate advancements in engineering and optimizing wave propagation channels, particularly for millimeter-wave communications.**

***Index Terms*—Metasurfaces, Electromagnetic diffraction, Harmonic analysis, Millimeter wave propagation, Surface impedance**

I. Introduction

The constant demand for increasing bandwidth and transfer rates has pushed wireless technologies towards higher-frequency bands. It is expected that prospective high-frequency mobile communications will use highly-directive and possibly scanning antennas to provide gain in the desired direction and compensate for the additional propagation losses. In addition, it will be desirable or even required to engineer the propagation environment and create additional channels that will avoid obstacles using fixed or reconfigurable intelligent surfaces (RIS) realizing anomalous reflection [1]. There are different methods to design metasurfaces [2] for anomalous reflection (e.g., [3]–[12]), with promising experimental results (e.g., [7], [8], [13]–[15]. In the design of such metasurfaces, it is typically assumed that the structures are infinitely large and illuminated by plane waves. However, in high-frequency telecommunications, such as those envisaged for 6G and beyond, the metasurface area may be smaller than the illuminated spot on the supporting wall. In this situation a considerable amount of power is reflected by the supporting wall, ultimately leading to unexpected scattering effects that can undermine the desired system performance.

We have recently developed an efficient method for design of anomalous reflectors and experimentally confirmed effective operation for D-band frequencies [16], [17]. The method is quite general, and it can be used for the design of periodic metasurfaces with arbitrary power distributions and arbitrarily selected phases among all propagating Floquet modes [17]. In this work, we will focus on metasurfaces for engineering beam splitting with both power and phase control. As an application example, we will use these metasurfaces to modify specular reflections from uniform walls surrounding metasurface panels. We show how a properly designed metasurface panel can modify scattering from a significantly wider area than the metasurface itself. Here, our focus is on fixed (static) metasurfaces, however, the results can be applied in the future also for reconfigurable reflectors. This study is most relevant for high-frequency (millimeter-wave and THz) systems, where signals are usually carried by narrow beams, and it is important to be able to engineer scattering patterns from illuminated objects, in order to ensure required coverage.

(Corresponding author: X. Wang) This work was supported in part by the European Commission through the Horizon 2020 (H2020) Artificial Intelligence Aided D-band Network for 5G Long Term Evolution (ARIADNE) project under grant 871464 and by the Academy of Finland under grant 345178.

S. Kosulnikov, F. S. Cuesta, and S. A. Tretyakov are with the Department of Electronics and Nanoengineering, Aalto University, FI-00076 Aalto, Finland. X. Wang is with the Institute of Nanotechnology, Karlsruhe Institute of Technology, Karlsruhe, Germany. (e-mail: sergei.2.kosulnikov@aalto.fi; francisco.cuestasoto@aalto.fi; xuchen.wang@kit.edu; sergei.tretyakov@aalto.fi).

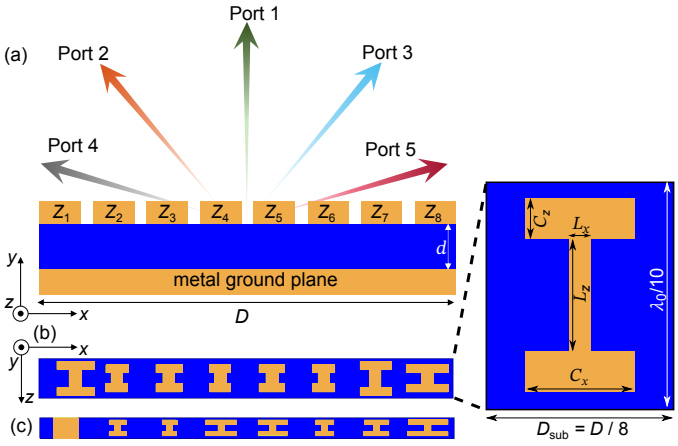

Fig. 1. Unit cells of the metasurfaces under study: (a) – schematic side view of a metasurface; (b) – top view of the implemented pattern for the 3-channel splitter; (c) – top view of the implemented 5-channel splitter (note that the left most subcell here is a conducting strip).

II. Design of Reflectors with Advanced Functionalities

At the first design step, the metasurface is modeled as a periodic array of supercells formed by impedance patches (Z_1, Z_2, $\cdots$, Z_K) on a grounded dielectric substrate, as shown on Fig. 1(a). We use the method presented in [17] to obtain the scattering amplitude and phase for all channels, each one corresponding to one of the propagating Floquet harmonics. The angle of reflection for the n-th harmonic θ_n is determined by the expression

$$\sin\theta_n = \sin\theta_\mathrm{i} + \frac{2\pi n}{kD}, \tag{1}$$

where θ_i is the incidence angle, k is the wavenumber of the incident wave, and D is the period (the supercell size) [18, Chapter 7]. Considering the scattering harmonics from $n = -N$ to $n = +N$, the amplitudes of the incident and reflected harmonics can be represented by $2N + 1$ dimensional arrays, $\mathbf{E}_\mathrm{i}$ and $\mathbf{E}_\mathrm{r}$, respectively. These arrays are related by the reflection matrix $\mathbf{R}$, which is a $2N + 1$ square matrix. The reflection matrix is determined by the substrate parameters and the discrete sheet-impedance values $Z_1, Z_2, \cdots Z_K$ of the impedance patches.

The metasurface design goal is to find a proper set of discrete impedance values for a given incidence and desired reflection harmonics. After the sheet impedances of the patches are known, they

can be realized as properly shaped metal patches. Since there is no analytical method to find the impedance values, we use a numerical optimization [17]. For excitations by a single TE-polarized plane wave, the incident-field vector $\mathbf{E}_\mathrm{i}$ can be written as an array with all zeros except for the central element which is equal to unity, $\mathbf{E}_\mathrm{i} = [0, \cdots, 0, 1, 0, \cdots, 0]^T$. Knowing the incident field $\mathbf{E}_\mathrm{i}$, the amplitudes of all scattered modes can be found as $\mathbf{E}_\mathrm{r} = \mathbf{R} \cdot \mathbf{E}_\mathrm{i}$, $\mathbf{E}_\mathrm{r} = [R_{-N} \cdots, R_{-1}, R_0, R_1, \cdots, R_N]^T$, where R_n refers to the complex amplitude of n-th scattering harmonic. The optimization target is to find a proper set of sheet impedance values Z_k to ensure that the calculated $\mathbf{E}_\mathrm{r}$ satisfies the design purposes.

For example, we can require that in the design of three-channel beam splitters of Fig. 1(a), the incident wave from port 2 is equally split to port 3 ($n = 0$) and port 1 ($n = -1$), with no power directed towards ports 4 and 5; and the reflection wave from port 1 has zero reflection phase. In this case, the incidence angle θ_i is defined as the angle between the directions of port 2 and port 1, and we set the following optimization goals:

$$|R_0| = 0.707, \quad |R_{-1}| = \frac{\sqrt{2}}{2}\sqrt{\frac{\cos\theta_\mathrm{i}}{\cos\theta_{-1}}}, \quad \arg(R_0) = 0. \qquad (2)$$

The first two objectives ensure that the power is equally distributed between ports 1 and 3. The third goal ensures zero reflection phase at port 3. We optimize the discrete impedance values $Z_1, Z_2, \cdots, Z_K$ (purely reactive) until the calculated reflection parameters meet the objectives. To find the optimal values of the sheet impedances, we use the optimization tool available in the MATLAB package. At each optimization step, MATLAB assumes an array of $Z_1, Z_2, \cdots, Z_K$ and calculates the reflected fields. Then, the cost is evaluated by summing up the differences between the desired and actual reflection parameters. Using the `MultiStart` and `fmincon` algorithms, MATLAB searches for the minimum value of the cost function in the multidimensional parameter space.

To illustrate versatile possibilities of multi-beam reflection control, we design four types of metasurfaces, namely: a perfect anomalous reflector, a three-channel splitter with zero specular reflection phase, an artificial magnetic conductor (AMC) working as a specular reflector with zero reflection phase, and a five-channel splitter with reflected waves towards two anomalous directions. Furthermore, we present actual implementations of the designed metasurfaces as arrays of "dog-bone" metal patches. We do not implement the anomalous reflector since an equivalent structure was already implemented and experimentally validated in Ref. [17]. The AMC is also straightforward to implement, as it allows a direct analytical solution and has been investigated in detail in many papers (see e.g. [19]).

In all considered examples, the structures operate at 144.75 GHz (the central frequency of the second D-band channel), and the oblique incidence is from $\theta_\mathrm{i} = 70^\circ$, as shown in Fig. 1(a). The periodic metasurface of the period D is discretized to $K = 8$ subcells. The metasurfaces are realized as three-layer structures made of a penetrable infinitely thin impedance sheet over a Quartz substrate with $\varepsilon_\mathrm{r} = 4.2$ and the loss tangent 0.005, see an illustration on Fig. 1(a). The substrate thickness is $d = 209.5$ μm, and the ground plane is made of copper.

A. Anomalous reflector

Our first reference structure is a perfect anomalous reflector. We set $D = \lambda_0/\sin\theta_\mathrm{i}$, $\theta_\mathrm{i} = 70^\circ$ (port 2) and optimize the structure to maximize the amplitude of the $n = -1$ reflected harmonic (port 1). The optimization objective is the value corresponding to perfect conversion of the incident power to this mode: $|R_{-1}| = \sqrt{\cos\theta_\mathrm{i}/\cos\theta_\mathrm{r}}$ [5], [6]. The optimization results in values $Z = [-132, -278, -187, -1215, -1099, -1008, -989, 50]j$ Ohm. We assume a finite thickness and realistic losses of the dielectric substrate, a finite conductivity of the background metal, and the patch arrays are modelled as penetrable impedance sheets (i.s.) using ANSYS HFSS. The corresponding scattering matrix $S_\mathrm{i.s.}$ reads (the values are rounded to the second digit)

$$|S_\mathrm{i.s.}| = \begin{bmatrix} 0.01 & \mathbf{0.99} & 0.01 \\ 0.99 & 0.00 & 0.02 \\ 0.01 & 0.02 & 0.98 \end{bmatrix}. \qquad (3)$$

Anomalous reflection from this infinite structure is almost perfect, with the efficiency $\eta_\mathrm{eff} = |S_{12}|^2 = 97.74\%$. The imperfections are caused mainly by losses in the dielectric substrate and in the copper ground plane.

TABLE I
DESIGN PARAMETERS OF THE IMPLEMENTED SPLITTERS.

	3 chan.	5 chan.		3 chan.	5 chan.
C_{x1}, μm	223	420	L_{x1}, μm	60	60
C_{x2}, μm	164	257	L_{x2}, μm	60	60
C_{x3}, μm	116	188	L_{x3}, μm	60	60
C_{x4}, μm	134	316	L_{x4}, μm	60	60
C_{x5}, μm	110	330	L_{x5}, μm	60	60
C_{x6}, μm	136	147	L_{x6}, μm	60	60
C_{x7}, μm	114	170	L_{x7}, μm	60	60
C_{x8}, μm	194	0	L_{x8}, μm	60	263
C_{z1}, μm	40	40	L_{z1}, μm	60	80
C_{z2}, μm	40	40	L_{z2}, μm	100	80
C_{z3}, μm	40	40	L_{z3}, μm	60	80
C_{z4}, μm	40	40	L_{z4}, μm	60	80
C_{z5}, μm	40	40	L_{z5}, μm	60	80
C_{z6}, μm	40	40	L_{z6}, μm	60	80
C_{z7}, μm	40	40	L_{z7}, μm	60	80
C_{z8}, μm	40	0	L_{z8}, μm	100	$\lambda_0/10$

B. Three-channel splitter

For this design, we keep the same periodicity D and θ_i. As a target, we request the optimization objective as defined in Eq. (2). The resulted sheet impedance vector reads $Z = [-611, -262, -911, -806, -948, -771, -951, -209]j$ Ohm. EM simulations result in the following scattering matrix:

$$S_\mathrm{i.s.} = \begin{bmatrix} 0.51\angle -24.6^\circ & \mathbf{0.69}\angle \mathbf{-114}^\circ & 0.49\angle 89.9^\circ \\ 0.69\angle 65.9^\circ & 0\angle -133^\circ & 0.69\angle -0.1^\circ \\ 0.49\angle -90.1^\circ & \mathbf{0.69}\angle \mathbf{-0.1}^\circ & 0.48\angle 23.5^\circ \end{bmatrix}. \qquad (4)$$

From this scattering matrix we see that the incident power is split between the 1st and 3rd ports very precisely, and the reflection phases towards the specular direction (S_{23} and S_{32}) are close to zero.

We use a procedure similar to that presented in Ref. [17] to find "dog-bone" meta-atom dimensions granting the desired sheet impedance values. This type of meta-atoms allows to achieve reliable angular stability, see e.g. [20]–[22]. The discretization step of the structure along the z-axis is $\lambda_0/10$. We first implement the local sheet impedances using "dog-bone" meta-atoms and then perform additional numerical tuning of the meta-atom parameters in order to equate the split powers and minimize the specular reflection phase. The optimized design parameters are presented in Table I (column "3 chan."), and the structural parameters are shown in the inset of Fig. 1. Worth noting that we shifted the first dog-bone element inside the subcell by 0.2 of the subcell period to improve the desired functionality. The overall top view of the implemented supercell is presented in Fig. 1(b). The scattering matrix of the implemented optimized infinite structure $S_\mathrm{imp}^\mathrm{opt}$ reads

$$S_{\text{imp}}^{\text{opt}} = \begin{bmatrix} 0.55\angle -30.3^\circ & \mathbf{0.64\angle -105^\circ} & 0.45\angle 92^\circ \\ 0.64\angle 75^\circ & 0.18\angle -115^\circ & 0.62\angle 0.53^\circ \\ 0.46\angle -88^\circ & \mathbf{0.62\angle 0.53^\circ} & 0.47\angle -8.48^\circ \end{bmatrix}. \quad (5)$$

This result confirms the desired performance. The power is nearly equally split, and the specular reflection phase is negligibly small. However, the retroreflection coefficient S_{22} grows up to 3.2%.

C. Artificial Magnetic Conductor

We proceed with the 3-port functionality [see Fig. 1(a)] to design an AMC, maximizing the amplitude of the $n = 0$ harmonic, with the target value $R_0 = 1$. The resulting sheet reactance is in accordance to that obtained from the equivalent transmission-line model of a homogeneous grid on a grounded substrate equals $Z_{1-8} = -472j$ Ohm. The scattering matrix resulting from EM simulations reads

$$S_{\text{i.s.}} = \begin{bmatrix} 0.99\angle -26.4^\circ & 0.00\angle -14.9^\circ & 0.00\angle -10.7^\circ \\ 0.00\angle 165^\circ & 0.00\angle 49.7^\circ & 0.97\angle 0.21^\circ \\ 0.00\angle 169^\circ & \mathbf{0.97\angle 0.21^\circ} & 0.00\angle 129^\circ \end{bmatrix}. \quad (6)$$

D. Splitting into two anomalous directions

In order to split the energy between two anomalous directions we double the periodicity of the structure, setting it to $D = 2\lambda_0/\sin\theta_{\text{i}}$. For illumination from $\theta_{\text{i}} = 70^\circ$, there are the following propagating reflected harmonic angles: $\theta_0 = 70^\circ$ (port 5), $\theta_{-1} = 28.024^\circ$ (port 3), $\theta_{-2} = 0^\circ$ (port 1), $\theta_{-3} = -28.024^\circ$ (port 2), $\theta_{-4} = -70^\circ$ (port 4). In this example, we define the target to equally split the incident power to the $n = -1$ and $n = -2$ anomalous scattering harmonics, which is equivalent to power incident from port 4 splitting between ports 3 and 1. The optimization objective is $|R_{-2}| = \sqrt{\frac{1}{2}\frac{\cos\theta_{\text{i}}}{\cos\theta_{-2}}}$, and $|R_{-1}| = \sqrt{\frac{1}{2}\frac{\cos\theta_{\text{i}}}{\cos\theta_{-1}}}$ resulting in $Z = [-110, -427, -662, -294, -265, -867, -750, 40]j$ Ohm. EM simulations give the scattering matrix

$$|S_{\text{i.s.}}| = \begin{bmatrix} 0.31 & 0.47 & 0.32 & \mathbf{0.69} & 0.29 \\ 0.47 & 0.65 & 0.44 & 0.00 & 0.39 \\ 0.32 & 0.44 & 0.32 & \mathbf{0.71} & 0.30 \\ 0.69 & 0.00 & 0.71 & 0.00 & 0.01 \\ 0.29 & 0.39 & 0.30 & 0.01 & 0.80 \end{bmatrix}.$$

This result confirms the desired functionality: $S_{14} \approx S_{34}$, whereas the other scattering parameters for illumination from port 4 are negligibly small. The geometrical parameters of the implemented dog-bone meta-atoms are presented in Table I in the column "5 chan.". The overall top view of the implemented structure is given in Fig. 1(c). The resulting scattering matrix from the EM simulation S_{imp} reads

$$|S_{\text{imp.}}| = \begin{bmatrix} 0.43 & 0.32 & 0.29 & \mathbf{0.61} & 0.38 \\ 0.32 & 0.57 & 0.34 & 0.18 & 0.52 \\ 0.29 & 0.34 & 0.40 & \mathbf{0.61} & 0.21 \\ 0.61 & 0.18 & 0.61 & 0.18 & 0.06 \\ 0.38 & 0.52 & 0.21 & 0.06 & 0.45 \end{bmatrix}. \quad (7)$$

The theoretical reflectance $|S_{14}|^2$ is expected to be 50% (even power splitting), but the simulations results form Eq. (7) shows it decays down to 37%, which results in efficiency of 74%.

III. Scattering Patterns of Metasurface Panels on Uniform Walls

In this section, we apply the developed metasurfaces to validate their scattering performance with the consideration of reflecting walls. We validate full-wave EM simulations with the previously developed theoretical model of scattering from the finite-sized metasurfaces

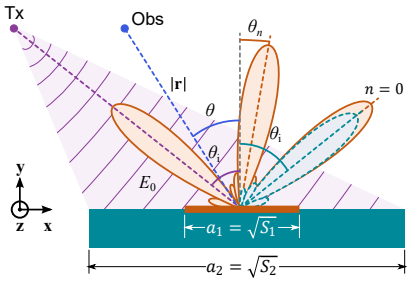

Fig. 2. Schematic of a metasurface of the area $S_1 = a_1^2$ on top of a uniform wall. The illuminated area equals $S_2 = a_2^2$. The scattering field at the observation point E_{scz} is result of the interference of the scattering produced by the metasurface with the one produced by the wall.

[23]. Finally, we analyze how these structures can be utilized for molding scattering towards specular direction.

Let us consider a metasurface with the supercell configuration of Fig. 1. If the metasurface pattern repeats infinitely, the scattering produced by plane-wave illumination is a combination of plane-wave Floquet harmonics with specular and non-specular propagation directions, following Eq. (1). In a more realistic scenario, illustrated in Fig. 2, the metasurface has a finite area $S_1 = a_1^2$, where a_1 is the metasurface side, and it is illuminated by a directive beam. We assume that in the far zone of the transmitting antenna the wavefront can be approximated by a plane wave. The metasurface is placed at a wall with homogeneous properties, and the illuminated surface area is $S_2 = a_2^2$ for simplicity, (approximating the beam shape as a square). For TE-polarized incidence (z-polarized in the present notations), the scattered field in the far zone E_{scz} follows the model of Ref. [24, Eq. (17)].

First, we validate the scattering performance of the finite-size array, comparing the full-wave simulation model with the theoretical model presented in Ref. [24], calculating the scattered electric field E_{scz} at $|\mathbf{r}| = 1$ m distance from the metasurface. These simulations are computationally demanding, therefore we use semi-analytical models, modeling patch arrays by sheet impedances and considering relatively small finite-size samples. We compare two cases: 1) when the illuminated area covers the metasurface only; 2) when the illumination covers the metasurface and a part of the surrounding reflecting wall. We consider the surrounding wall as a PEC (Perfect Electric Conductor) boundary as the most extreme case with the reflection coefficient $R_{\text{wall}} = -1$. However, the used theoretical model is applicable for any value of the wall reflection coefficient [23], [24]. The model of Refs. [23], [24] can also be extended considering the roughness of the wall, by either modeling it using a set of multiple Floquet modes or through measurement data, but such implementations are out of the scope of this work. The total sizes of the simulated structures are $a_1 = 8D$ and $a_2 = 16D$ (with an illuminated wall) or $S_2 = S_1$ (only the metasurface is illuminated), in accordance with the model in Ref. [24]. Similarly to the semi-analytical EM simulations provided for the infinitely periodic structures in Sec. II, the finite metasurfaces are modeled in ANSYS HFSS as three-layer structures made of penetrable impedance sheets over a Quartz substrate, and the ground plane made of copper. These results are presented in Fig. 3.

Next, we utilize the same theoretical model of Ref. [24] to analyse scattering from these four metasurfaces toward the specular region. To this end, we fix the illuminated spot area to $S_2 = a_2^2 = 100\lambda_0 \times 100\lambda_0$ and calculate the scattered fields at $|\mathbf{r}| = 1$ m distance in a narrow angular sector close to the specular direction. Similarly to our full-wave simulations, the metasurfaces are located at a PEC wall. The structures in this theoretical analysis are of a

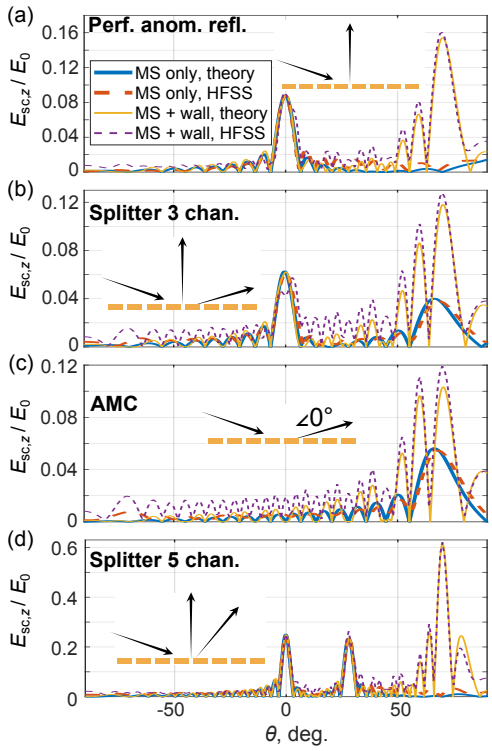

Fig. 3. Normalized scattered electric field E_{scz}/E_0 at 1 m distance from the metasurfaces under plane-wave illumination at $\theta_{\mathrm{i}} = -70^{\circ}$ calculated using the theoretical model of Ref. [24] and EM simulations: (a) – perfect anomalous reflector; (b) – splitter 3-channel; (c) – perfect specular reflector; (d) – splitter 5-channel. For every case we compare scattering from the metasurface only and from the metasurface surrounded by a PEC wall. Note that in case (d) the areas S_1 and S_2 are larger, because the period D is twice as large as compared to cases (a-c). Schematic insets demonstrate the corresponding targeted ideal metasurface functionality.

larger electrical size to be closer to prospective application scenarios in indoor environments. The main goal here is to study how the specular reflection from the wall is modified due to reflections from metasurface panels of different sizes in the range $0 \leq a_1 \leq a_2$. These results are presented in Fig. 4.

A. Anomalous reflector

The first structure under consideration is an anomalous reflector, which is a three-port structure where the amplitude of the reflected mode $n = -1$ is maximized, as represented in the insert of Fig. 3(a). The far-field scattering pattern of this metasurface panel is shown in Fig. 3(a). The theoretical result from the model of Ref. [24] and considering only the presence of the metasurface (without illumination of the surrounding PEC wall) is marked as "MS only, theory". The corresponding result from the EM simulation of the same finite metasurface is marked as "MS only, HFSS". In a realistic scenario, the total scattered field at the receiver position is a combination of the power scattered by the metasurface and the power reflected from the wall. Therefore, the other two lines marked as "MS + wall" show the case when the illuminated area covers also a part of the surrounding wall. One can see from the results that the anomalous reflection towards 0° remains close to the estimated, as the metasurface area remains the same. There is only some modification of side-lobe scattering. However, significant scattering towards the specular direction appears for the case when the surrounding wall is illuminated.

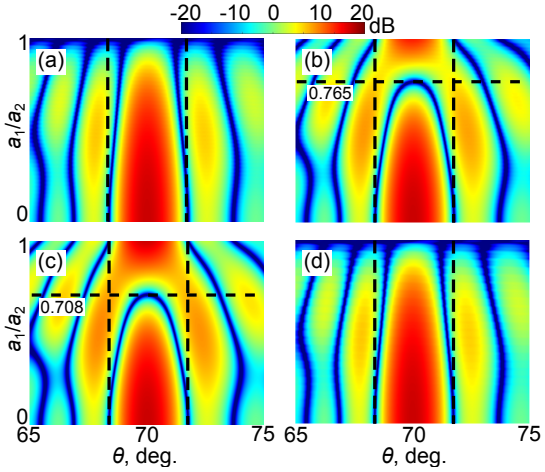

Fig. 4. Scattering pattern in a small sector around the specular reflection angle. The structures are described in Sec. III. The scattered field is calculated using the model of Ref. [24]: (a) – perfect anomalous reflector; (b) – three-channel splitter with 0° specular reflection phase; (c) – perfect specular reflector with 0° specular reflection phase; and (d) – five-channel splitter into two anomalous directions. The vertical black dashed lines show the initial width of the specular lobe, and the Horizontal dashed lines show the ratio region where the specular scattering is suppressed.

As observed in Ref. [24], the amplitudes of the scattered fields produced by the metasurface and the illuminated wall are proportional to their areas. Results in Fig. 4(a) show how the field intensity in the specular direction $\theta_0 = 70^{\circ}$ is affected by the metasurface size for varying illuminated area of the wall. Vertical black dashed lines show the initial width of the specular lobe, which is similar for all four considered cases, when the metasurface is absent. An increase of the metasurface area leads to stronger destructive interference in the specular reflection, resulting in complete suppression when the metasurface size a_1 is equal to the illuminated area of the wall. However, in this example, modifications of the specular beam pattern are small, because only weak side-lobe radiation from the metasurface interferences with the wall reflection.

B. Three-channel splitter

The designed three-port splitter [see Fig. 3(b)] divides the scattered power equally between the specularly reflected mode $n = 0$ and the anomalously reflected mode $n = -1$, producing specular reflection with zero phase delay. The metasurface performs as intended, as seen in Fig. 3(b). Specular reflection from the surrounding wall is in this case out of phase with the reflection from the metasurface, as revealed in the results from Fig. 4(b). The results are very different from the anomalous reflector case, due to destructive interference between specular reflections from the metasurface and the surrounding wall. The specularly reflected lobe degrades faster, compared to the anomalous reflector, and its width shrinks. The most noticeable effect is found at $a_1/a_2 \approx 0.765$ (marked with horizontal black line) where the metasurface and the illuminated part of the wall reflect the same power towards the specular direction, resulting in a pattern null at θ_{i}. At the same time, amplitudes of the side lobes around the specular direction increase, producing diffuse scattering effects. Importantly, launching similar interference beams by one metasurface can be difficult or even not practically possible. This is because launching waves into two or more arbitrary directions may require an impractically large period of the array. Thus, the proposed method of using interference is a useful addition to methods of controlling reflections.

C. Artificial magnetic Conductor

Even stronger effects of PEC wall-reflection control are seen if the metasurface is designed as an artifical magnetic conductor. To calculate the corresponding patterns, we set $R_{n\neq 0} = 0$ and $R_{n=0} = 1$ in the model of Ref. [24], which gives the scattering pattern presented in Fig. 3(c). The results of the equivalent analysis as for the anomalous reflector with varying a_1/a_2 are presented in Fig. 4(c). The effect of specular scattering lobe vanishing and side-lobe enhancement occurs now faster as compared to the three-channel power splitter. All the incident power at the metasurface area is used to affect the reflection from the illuminated part of the wall. The null in the specular reflection occurs at $a_1/a_2 \approx 0.708$. Thus, the metasurface controls reflection from the area that is in total about twice as large as the metasurface itself ($S_2 \approx 2S_1$).

D. Splitting into two anomalous directions

The last structure analysed in this work is a five-channel metasurface, shown in Fig. 1(c). Here, we maximize scattering into two anomalous directions for oblique-incidence illumination (the $n = -1$ and $n = -2$ harmonics). Reflection into the $n = -1$ harmonic produces non-specular scattering in the direction $\theta_{-1} = \operatorname{asin}(0.5 \sin\theta_{\mathrm{i}})$. According to Eq. (1), this corresponds to radiating towards $\theta_{-1} \approx 28^\circ$ in the case that $\theta_{\mathrm{i}} = 70^\circ$. The other anomalous reflection beam $n = -1$ is in the normal direction. Reflections from the metasurface into the specular directions are small, similarly to the three-channel splitter, but one of the two reflected beams can be used to control reflections from the supporting wall if the wall is not flat.

The results in Fig. 3(d) with only the metasurface demonstrate the intended properties of the structure. As is seen from Fig. 4(d), there is very little effect of the metasurface on reflections into the specular direction from this flat wall. This is similar to the anomalous reflector, with minor changes in the corresponding values of $a_1 \to a_2$ due to somewhat different metasurface scattering into the side-lobes. This is expected, because the design of both these metasurfaces minimizes any possible reflections towards the specular direction.

IV. Conclusions

In this paper we discussed possibilities to mold reflected fields from illuminated spots on uniform walls using advanced anomalous reflectors. The study is relevant to millimeter-wave telecommunications where directive antennas are used and the propagation environment does not offer rich diffuse scattering. In the considered examples we introduced metasurfaces that create several controllable reflected beams and enhance diffuse scattering. Engineering the multichannel behavior of the considered structures allows us to effectively shape reflections into the specular direction and into the side-lobes. In particular, it was shown that metasurfaces can effectively modify specular reflections from surrounding walls, redirecting a certain part of the specularly scattered power into secondary lobes.

The paper describes the complete design process, from the definition of the desired functionality to finding the appropriate shape and dimensions of meta-atoms and finally to estimations of the far-field scattering pattern of the metasurface placed at a uniform wall. In the considered examples we assumed perfect conductivity of the supporting wall, which required zero-phase specular reflection from metasurface in order to realize destructive interference. However, the demonstrated possibility to arbitrarily engineer the reflection amplitude and phase for all propagating Floquet harmonics allows us to achieve the same effects for walls with arbitrary reflection coefficients. Results of an experimental test of a millimeter-wave anomalous reflector designed using the developed method can be found in [17]. The presented analytical model in combination with the algorithm for implementation of the metasurface profile allows us to engineer the properties of reflected beams as required for both anomalous reflections and desired interference with the wall reflections, defined by the complex-valued reflection coefficient of the wall. Worth noting that other illumination parameters, as e.g. beamwidth and/or source directivity can be incorporated using the related illumination models (see [23], [24]). In this work, we set the walls material to PEC and assume uniform illumination for demonstration purposes, considering the most extreme case when reflection from the surrounding wall is the strongest. Diffusion due to wall roughness also can play an important role, but developing means to control also that would require more technical investigations that are out of the scope of this work.

The results bring an alternative path for metasurface applications, where the desired scattering is produced not only by the metasurface itself but also due to engineered interference with the surrounding environment. We believe that these results are useful for optimization of propagation channels in prospective telecommunication systems utilizing high-frequency bands. Reconfigurable versions of similar multi-channel reflectors can further enhance application scenarios of engineered surfaces.

References

[1] M. Di Renzo, A. Zappone, M. Debbah, M.-S. Alouini, C. Yuen, J. de Rosny, and S. Tretyakov, "Smart radio environments empowered by reconfigurable intelligent surfaces: How it works, state of research, and the road ahead," *IEEE J. Sel. Areas Commun.*, vol. 38, no. 11, pp. 2450–2525, 2020.

[2] S. B. Glybovski, S. A. Tretyakov, P. A. Belov, Y. S. Kivshar, and C. R. Simovski, "Metasurfaces: From microwaves to visible," *Phys. Rep.*, vol. 634, pp. 1–72, 2016.

[3] R. D. Javor, X.-D. Wu, and K. Chang, "Design and performance of a microstrip reflectarray antenna," *IEEE Trans. Antennas Propag.*, vol. 43, no. 9, pp. 932–939, 1995.

[4] D. M. Pozar, S. D. Targonski, and H. Syrigos, "Design of millimeter wave microstrip reflectarrays," *IEEE Trans. Antennas Propag.*, vol. 45, no. 2, pp. 287–296, 1997.

[5] A. Epstein and G. V. Eleftheriades, "Synthesis of passive lossless metasurfaces using auxiliary fields for reflectionless beam splitting and perfect reflection," *Phys. Rev. Lett.*, vol. 117, no. 25, p. 256103, 2016.

[6] V. S. Asadchy, M. Albooyeh, S. N. Tcvetkova, A. Díaz-Rubio, Y. Ra'di, and S. Tretyakov, "Perfect control of reflection and refraction using spatially dispersive metasurfaces," *Phys. Rev. B*, vol. 94, no. 7, p. 075142, 2016.

[7] A. Díaz-Rubio, V. S. Asadchy, A. Elsakka, and S. A. Tretyakov, "From the generalized reflection law to the realization of perfect anomalous reflectors," *Sci. Adv.*, vol. 3, no. 8, p. e1602714, 2017.

[8] V. S. Asadchy, A. Wickberg, A. Díaz-Rubio, and M. Wegener, "Eliminating scattering loss in anomalously reflecting optical metasurfaces," *ACS Photonics*, vol. 4, no. 5, pp. 1264–1270, 2017.

[9] Y. Radi, D. L. Sounas, and A. Alù, "Metagratings: Beyond the limits of graded metasurfaces for wave front control," *Phys. Rev. Lett.*, vol. 119, no. 6, 2018.

[10] V. Popov, F. Boust, and S. N. Burokur, "Controlling diffraction patterns with metagratings," *Phys. Rev. Appl.*, vol. 10, no. 1, p. 011002, 2018.

[11] D.-H. Kwon, "Planar metasurface design for wide-angle refraction using interface field optimization," *IEEE Antennas Wireless Propag. Lett.*, vol. 20, no. 4, pp. 428–432, 2021.

[12] J. Budhu and A. Grbic, "Perfectly reflecting metasurface reflectarrays: Mutual coupling modeling between unique elements through homogenization," *IEEE Trans. Antennas Propag.*, vol. 69, no. 1, pp. 122–134, Jan. 2021.

[13] J.-B. Gros, V. Popov, M. A. Odit, V. Lenets, and G. Lerosey, "A reconfigurable intelligent surface at mmWave based on a binary phase tunable metasurface," *IEEE Open J. Commun. Soc.*, vol. 2, pp. 1055–1064, 2021.

[14] H. Lin, W. Yu, R. Tang, J. Jin, Y. Wang, J. Xiong, Y. Wu, and J. Zhao, "A dual-band reconfigurable intelligent metasurface with beam steering," *J. Phys. D: Appl. Phys.*, vol. 55, no. 24, p. 245002, Mar. 2022.

[15] M. Barbuto, A. Al, F. Bilotti, and A. Toscano, "Composite vortex manipulation as a design tool for reflective intelligent surfaces," *IEEE Antennas Wirel. Propag. Lett.*, pp. 1–5, 2023, Early Access.

[16] X. Wang, A. Díaz-Rubio, and S. A. Tretyakov, "Independent control of multiple channels in metasurface devices," *Phys. Rev. Appl.*, vol. 14, no. 2, p. 024089, 2020.

[17] S. Kosulnikov, X. Wang, and S. A. Tretyakov, "Discrete impedance metasurfaces for 6G wireless communications in D-band," 2023, *arXiv:2302.07313*.

[18] A. Ishimaru, *Electromagnetic Wave Propagation, Radiation, and Scattering*. Prentice Hall, 1991.

[19] D. Sievenpiper, L. Zhang, R. F. Broas, N. G. Alexopolous, and E. Yablonovitch, "High-impedance electromagnetic surfaces with a forbidden frequency band," *IEEE Trans. Microw. Theory Tech.*, vol. 47, no. 11, pp. 2059–2074, 1999.

[20] C. Simovski, P. de Maagt, and I. Melchakova, "High-impedance surfaces having stable resonance with respect to polarization and incidence angle," *IEEE Trans. Antennas Propag.*, vol. 53, no. 3, pp. 908–914, 2005.

[21] A. Vallecchi and A. G. Schuchinsky, "Entwined planar spirals for artificial surfaces," *IEEE Antennas Wirel. Propag. Lett.*, vol. 9, pp. 994–997, 2010.

[22] J. Shabanpour and C. R. Simovski, "Angular and polarization stability of broadband reconfigurable intelligent surfaces of binary type," *IEEE Access*, vol. 10, pp. 126 253–126 268, 2022.

[23] S. Kosulnikov, F. Cuesta, X. Wang, and S. Tretyakov, "Simple link-budget estimation formulas for channels including anomalous reflectors," *IEEE Trans. Antennas Propag.*, 2023.

[24] A. Díaz-Rubio, S. Kosulnikov, and S. Tretyakov, "On the integration of reconfigurable intelligent surfaces in real-world environments: A convenient approach for estimation reflection and transmission," *IEEE Antennas Propag. Mag.*, pp. 2–13, 2022.